On Zero-Forcing Equalization for Short-Filtered Multicarrier Faster-than-Nyquist Signaling

Albert Abelló [*], Damien Roque[†], Cyrille Siclet[‡] and Alexandre Marquet[‡]

[*]Eutelsat S.A., 75015 Paris, France
email: aabellob@eutelsat.com
[†]Institut Supérieur de l'Aéronautique et de l'Espace (ISAE-SUPAERO), Université de Toulouse, 31055 Toulouse, France
email: damien.roque@isae-supaero.fr
[‡]GIPSA-Lab, Univ. Grenoble Alpes, F-38000 Grenoble, France
CNRS, GIPSA-Lab, F-38000 Grenoble, France
email: {cyrille.siclet,alexandre.marquet}@gipsa-lab.fr

Abstract—Within the context of faster-than-Nyquist signaling, a low-complexity multicarrier system based on short-length filters and zero-forcing turbo equalization is introduced. Short-length filters allow a reduced-size block processing while zero-forcing equalization allows a linear reduced-complexity implementation. Furthermore, rectangular and out-of-band energy minimization pulse shaping demonstrates competitive performance results over an additive white Gaussian noise channel while keeping a lower computational cost than other multicarrier faster-than-Nyquist systems.

Index Terms—Multicarrier, faster-than-Nyquist, zero-forcing, short-length filters, turbo equalization.

I. Introduction

The idea of faster-than-Nyquist (FTN) transmission was introduced by J. E. Mazo in 1975 [1] in order to improve spectral efficiency (beyond the Nyquist rate) while keeping a constant number of bits per symbol. This transmission technique yields inter-pulse-interference (IPI) so that non-linear receivers are required in order to perfectly reconstruct the sequence of transmitted symbols [2]. This extra computational load compared with orthogonal systems has prevented the use of FTN techniques for a while.

More recently, technological improvements combined with joint equalization/decoding methods [3] have renewed interest in FTN systems [4]. The concept has also been extended to multicarrier modulations, where IPI arises in the time-frequency plane [5]. Practical realizations have shown good performance results [6]–[8] and make multicarrier techniques attractive for a wide variety of applications such as fifth generation (5G) mobile communications [9]. However, it is still challenging to find a good trade-off between complexity, spectral efficiency and bit-error-rate (BER) performance.

In this work, we focus on a low-complexity receiver based on short-length filters and a zero-forcing turbo equalizer. On the one hand, the use of short-length filters allows to combine (non-rectangular) pulse shaping operation along with M-size block processing (where M is the number of subcarriers) as

an FTN extension of [10]. On the other hand, rectangular and out-of-band energy minimization pulse shapes demonstrate competitive performance results in the context of an additive white Gaussian noise (AWGN) channel while keeping a lower computational cost than other FTN systems mentioned before.

Our article is organized as follows. Section II describes the input-output relations of a linear FTN multicarrier system in the particular case of short-length filters. Section III presents the structure of the zero-forcing turbo equalizer. Section IV evaluates our system performance over the AWGN channel by means of simulations and following the filters design in [11]. Finally, our conclusions are stated in Section V.

II. System input-output relations

In this Section, we first present the input-output relations of a linear multicarrier system operating in an FTN context. Secondly, we focus on the particular case of short-length filters in order to achieve a low-complexity implementation.

A. Discrete-time multicarrier system

Let $\{c_{m,n}\}_{(m,n)\in \mathbf{Z}^2} \subset \mathbf{C}$ be a sequence of symbols to be transmitted, taken in a finite constellation. Symbols are assumed to be independent and identically distributed (i.i.d.), such that $\mathrm{E}\{c_{m,n}c_{m',n'}\} = \sigma_c^2 \delta_{m,m'}\delta_{n,n'}$, $\forall(m,n),(m',n') \in \mathbf{Z}^2$, where $\mathrm{E}\{\cdot\}$ is the expectation operator and δ is the Kronecker delta. We also denote $g[k] \in \mathbf{R}$ ($k \in \mathbf{Z}$) the transmission pulse shape, of finite energy.

As shown in [12], the output of a discrete time multicarrier transmitter is given by

$$s[k] = \sum_{(m,n)\in \mathbf{Z}^2} c_{m,n}g[k - nN]e^{j2\pi \frac{m}{M}k}, \quad k \in \mathbf{Z} \quad (1)$$

where M and N are strictly positive integers such that $1/M$ and N represent elementary symbol spacing in the frequency and time domains, respectively (Fig. 1). As a consequence, the signaling density of the system is given by $\rho = M/N$. It can be shown [13, Chapter 9] that transmission systems can be classified into two categories:

- if $\rho \leq 1$, there are biorthogonal systems that allow symbols to be perfectly reconstructed through a linear receiver;
- if $\rho > 1$, biorthogonal systems are not achievable but if one further assumes that symbols are taken from a finite alphabet, they may still be recovered using a non-linear receiver [14].

In our study, we focus on the latter case that can be seen as a generalization of single-carrier FTN systems in the sense that their signaling density overrides the IPI-free transmission rule. In usual applications, a finite set of non-null symbols is generally considered such that $\{c_{m,n} = 0\}_{(m,n) \notin \{0,...,M-1\} \times \{0,...,K-1\}}$ where K is a strictly positive integer representing the number of multicarrier symbols to be transmitted.
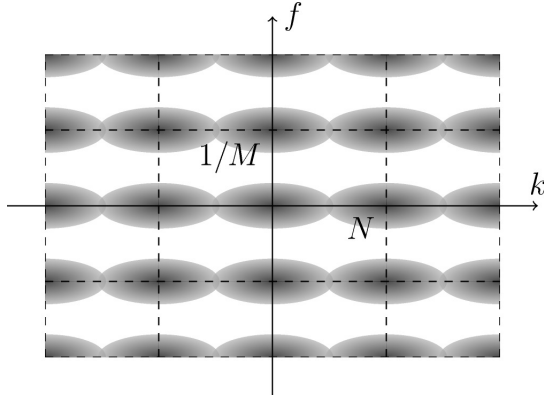

Fig. 1. Representation of the transmitted signal in the time-frequency plane.

In an AWGN channel, the received signal is denoted $r[k] = s[k] + n[k]$ where $n[k]$ is a circular Gaussian random process with zero-mean and variance σ_n^2.

Let $\check{g}[k] \in \mathbf{R}$ ($k \in \mathbf{Z}$) be the reception pulse shape, of finite energy. The output of the discrete time multicarrier receiver is given by

$$\tilde{c}_{p,q} = \sum_{k \in \mathbf{Z}} r[k]\check{g}[k - qN]e^{-j2\pi \frac{p}{M} k}, \quad (p,q) \in \mathbf{Z}^2 \quad (2)$$

$$= \underbrace{c_{p,q} A_{p,q,p,q}}_{\text{Useful signal}} + \underbrace{\sum_{(m,n) \neq (p,q)} c_{m,n} A_{m,n,p,q}}_{\text{Interference}} + \underbrace{z_{p,q}[k]}_{\text{Noise}} \quad (3)$$

with

$$A_{m,n,p,q} = \sum_{k \in \mathbf{Z}} g[k - nN]\check{g}[k - qN]e^{j2\pi \frac{(m-p)}{M} k}, \quad (4)$$

$$z_{p,q}[k] = \sum_{k \in \mathbf{Z}} n[k]\check{g}[k - qN]e^{-j2\pi \frac{p}{M} k}. \quad (5)$$

In the FTN case, since $\rho > 1$, we have necessarily $A_{m,n,p,q} \neq \delta_{m,p}\delta_{n,q}$ [14].

It is also interesting to mention that causality of the system has not been taken into account in the previous relations for the sake of brevity and without loss of generality in terms of system performance. However, the reader concerned by the topic might refer to [15].

B. Short-length filters and limited interference

There are several reasons to keep generators $g[k]$ and $\check{g}[k]$ as short as possible, for instance to reduce the computational complexity of the transmitter and receiver, to lower the reconstruction delay of the causal system or to limit interference in the time domain.

To serve this purpose, we consider a finite number M of subcarriers and we focus our analysis on short-length filters, namely $g[k] = \check{g}[k] = 0$ for $k < 0$ or $k > M-1$. Furthermore, we set $\rho < 2$ in order to limit interference to the contribution of two successive blocks of M symbols.

At the transmitter side, it is interesting to show that input blocks $\mathbf{c}_n = [c_{0,n}, \ldots, c_{M-1,n}]^{\mathrm{T}}$ of length M lead to output blocks $\mathbf{s}_l = [s_l[0], \ldots, s_l[N-1]]^{\mathrm{T}}$ of length N plus interblock interference, with $\cdot^{\mathrm{T}}$ the transpose operator. This can be done by setting $k = i + lN$ in (1) with $i, l \in \mathbf{Z}$ and denoting $s_l[i] = s[i + lN]$, such that the transmitter output can be rewritten as

$$s_l[i] = \begin{cases} C_l[i]g[i] \\ \quad + C_{l-1}[i+N]g[i+N], & \text{if } 0 \leq i \leq M - N - 1, \\ C_l[i]g[i], & \text{if } M - N \leq i \leq N - 1 \end{cases} \quad (6)$$

with

$$C_l[i] = \sum_{m=0}^{M-1} c_{m,l}e^{j2\pi \frac{m}{M}(i+nN)}. \quad (7)$$

A matrix form of (6) can be derived if we define $\mathbf{F}$ with $F[k,l] = 1/\sqrt{M}\exp(-j2\pi k(l + nN)/M)$, $0 \leq k,l \leq M - 1$, the inverse discrete Fourier transform matrix; $\mathbf{D}_g = \mathrm{diag}(g[0], \ldots, g[M-1])$, the pulse shaping matrix; $\mathbf{P}$ a projection matrix of size $M \times M$ such that

$$\mathbf{P} = \left[\begin{array}{c|c} \mathbf{0}_{M \times N} & \mathbf{I}_{M-N} \\ & \mathbf{0}_{N \times (M-N)} \end{array} \right] \quad (8)$$

where $\mathbf{I}$ and $\mathbf{0}$ represent identity and null matrices, respectively ; $\mathbf{T}$, a truncation matrix of size $N \times M$ with

$$\mathbf{T} = \left[\begin{array}{c|c} \mathbf{I}_N & \mathbf{0}_{N \times (M-N)} \end{array} \right]. \quad (9)$$

Finally, we obtain the expression of the lth transmitted block:

$$\mathbf{s}_l = \mathbf{T}\mathbf{D}_g\mathbf{F}^{\mathrm{H}}\mathbf{c}_l + \mathbf{T}\mathbf{P}\mathbf{D}_g\mathbf{F}^{\mathrm{H}}\mathbf{c}_{l-1} \quad (10)$$

where $\cdot^{\mathrm{H}}$ represents the conjugate transpose operator.

At the receiver side, it can conversely be shown that an input block $\mathbf{r}_q = [r_q[0], \ldots, r_q[N-1]]^{\mathrm{T}}$ of length N leads to an output block $\tilde{\mathbf{c}}_q = [\tilde{c}_{0,q}, \ldots, \tilde{c}_{M-1,q}]^{\mathrm{T}}$ of length M. This can be done by setting $r_q[k] = r[k + qN]$ with $k, q \in \mathbf{Z}$ such that (2) can be rewritten as

$$\tilde{c}_{p,q} = \sum_{k=0}^{M-1} \tilde{C}_q[k]e^{-j2\pi \frac{p}{M}(k+qN)} \quad (11)$$

with

$$\tilde{C}_q[k] = \begin{cases} \check{g}[k]r_q[k], & \text{if } 0 \leq k \leq N - 1, \\ \check{g}[k]r_{q+1}[k - N], & \text{if } N \leq k \leq M - 1. \end{cases} \quad (12)$$

A matrix form of (11) can be derived if we define $\mathbf{D}_{\breve{g}} = \mathrm{diag}(\breve{g}[0], \ldots, \breve{g}[M-1])$ the pulse shaping matrix such that

$$\tilde{\mathbf{c}}_q = \mathbf{F}\mathbf{D}_{\breve{g}}\left(\mathbf{T}^{\mathrm{T}}\mathbf{r}_q + \mathbf{P}^{\mathrm{T}}\mathbf{T}^{\mathrm{T}}\mathbf{r}_{q+1}\right). \qquad (13)$$

III. ZERO-FORCING EQUALIZATION OVER AN AWGN CHANNEL

As we stated in Section II, we limit interference to the contribution of two successive blocks of M symbols such that the block $\tilde{\mathbf{c}}_q$ at the output of the demodulator is affected by the last $M-N$ symbols of $\tilde{\mathbf{c}}_{q-1}$ and the first $M-N$ symbols of $\tilde{\mathbf{c}}_{q+1}$ (Fig. 2).
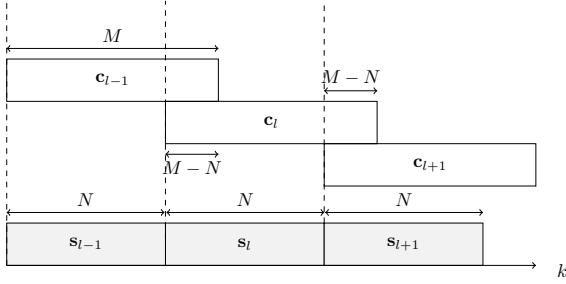

Fig. 2. Illustration of the interference pattern between consecutive blocks.

In such conditions, we can build a low-complexity equalizer using *a priori* information from a decoder. The turbo equalizer's iterative scheme would therefore consist of a linear equalizer performing zero-forcing interference cancelation on the qth block after subtracting interference caused by the $(q-1)$th and $(q-1)$th blocks. Such an interference cancellation is aided by the forward error correction decoder. The complete transmitter and receiver block diagram is depicted in Figure 3.
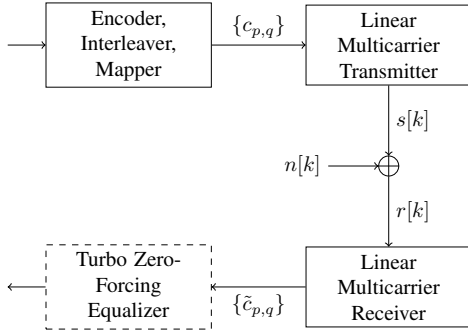

Fig. 3. Multicarrier system block diagram.

To derive the zero-forcing equalizer in the short-length filters hypothesis, we develop (13) considering the AWGN channel:

$$\tilde{\mathbf{c}}_q = \mathbf{F}\mathbf{D}_{\breve{g}}\Big[\mathbf{T}^{\mathrm{T}}(\mathbf{T}\mathbf{D}_g\mathbf{F}^{\mathrm{H}}\mathbf{c}_q + \mathbf{T}\mathbf{P}\mathbf{D}_g\mathbf{F}^{\mathrm{H}}\mathbf{c}_{q-1}) +$$
$$\mathbf{P}^{\mathrm{T}}\mathbf{T}^{\mathrm{T}}(\mathbf{T}\mathbf{D}_g\mathbf{F}^{\mathrm{H}}\mathbf{c}_{q+1} + \mathbf{T}\mathbf{P}\mathbf{D}_g\mathbf{F}^{\mathrm{H}}\mathbf{c}_q)\Big] + \mathbf{z}_q \qquad (14)$$

where $\mathbf{z}_q = [z_q[0], \ldots, z_q[M-1]]^{\mathrm{T}}$ is the qth block of noise samples at the demodulator's output with $z_q[k] = z[k+qN]$. If we note that $\mathbf{T}^{\mathrm{T}}\mathbf{T} + \mathbf{P}^{\mathrm{T}}\mathbf{T}^{\mathrm{T}}\mathbf{T}\mathbf{P} = \mathbf{I}_M$, we can rewrite (14) such that

$$\tilde{\mathbf{c}}_q = \mathbf{H}_q\mathbf{c}_q + \mathbf{H}_{q-1}\mathbf{c}_{q-1} + \mathbf{H}_{q+1}\mathbf{c}_{q+1} + \mathbf{z}_q \qquad (15)$$

where

$$\mathbf{H}_q = \mathbf{F}\mathbf{D}_{\breve{g}}\mathbf{D}_g\mathbf{F}^{\mathrm{H}},$$
$$\mathbf{H}_{q-1} = \mathbf{F}\mathbf{D}_{\breve{g}}\mathbf{T}^{\mathrm{T}}\mathbf{T}\mathbf{P}\mathbf{D}_g\mathbf{F}^{\mathrm{H}},$$
$$\mathbf{H}_{q+1} = \mathbf{F}\mathbf{D}_{\breve{g}}\mathbf{P}^{\mathrm{T}}\mathbf{T}^{\mathrm{T}}\mathbf{T}\mathbf{D}_g\mathbf{F}^{\mathrm{H}}. \qquad (16)$$

If we denote $\bar{\mathbf{c}}_{q-1}$ and $\bar{\mathbf{c}}_{q+1}$ the estimation at the equalizer's input of $\mathbf{c}_{q-1}$ and $\mathbf{c}_{q+1}$ respectively, we can derive the zero-forcing equalizer's output $\hat{\mathbf{c}}_q$:

$$\hat{\mathbf{c}}_q = \mathbf{H}_q^{-1}(\tilde{\mathbf{c}}_q - \mathbf{H}_{q-1}\bar{\mathbf{c}}_{q-1} - \mathbf{H}_{q+1}\bar{\mathbf{c}}_{q+1}) \qquad (17)$$

where the inversion of $\mathbf{H}_q$ yields a computational complexity of $O(M\log_2 M)$. The turbo equalizer complete scheme is depicted in Figure 4. The decoder log-likelihood ratios (LLRs) $\mathbf{L}_A^{(\mathrm{eq})}$ are symbol-converted to produce the *a priori* estimations $\bar{\mathbf{c}}_{q-1}$ and $\bar{\mathbf{c}}_{q+1}$ [16]. These two blocks are then linearly filtered and used in the interference cancelation process before being converted back to LLRs $\mathbf{L}_E^{(\mathrm{eq})}$. The iterative process includes interleaving and extrinsic information transfer between constituent blocks of the turbo equalizer to reduce direct feedback and avoid local convergence.
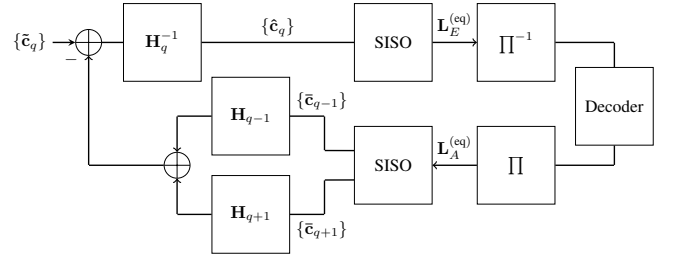

Fig. 4. Block diagram of the zero-forcing turbo equalizer.

IV. SIMULATIONS OVER AN AWGN CHANNEL

We present in this section BER performance as well as EXtrinsic Information Transfer (EXIT) simulations [17] for the transceiver described in Sections II and III.

The system performs rate-$1/2$ convolutional encoding with generator polynomials $[7,5]_8$ at the transmitter side and uses a random interleaver. Symbols are i.i.d. and follow a binary phase-shift keying (BPSK) mapping. At the receiver side, iterative zero-forcing equalization and *maximum a posteriori* (MAP) decoding is performed, as described in Section III. The turbo equalizer block contains K blocks of M symbols. We analyze the impact of pulse shaping of length M by means of rectangular (Rect) and non-rectangular out-of-band energy (OBE) minimization filters [11] (Fig. 5).

System BER performance for $\rho = 1.5$, (*i.e.*, 50% spectral efficiency gain) are shown in Figure 6, with E_b the energy

per bit and N_0 the noise power spectral density. We observe that rectangular pulses provide better performance results than OBE pulse shapes. One notes the fact that rectangular pulses weight equally the $2N - M$ non-interferent and the $M - N$ interferent symbols. On the other hand, OBE pulses yield a decay on the $M - N$ interferent symbols of a multicarrier block (Fig. 5) so that these interferent symbols are penalized by a lower signal-to-noise ratio than the non-interferent ones. In the frame of the AWGN channel considered here, since noise affects with the same power all transmitted symbols, OBE shaping can be seen as a non-desired water filling on the $M - N$ interferent symbols. As a consequence, the IPI-cancellation scheme is compromised at low E_b/N_0 values and explains worse BER performance for OBE pulse shaping than for rectangular pulse shaping. However, good performance results are obtained by means of the short-length filters assumption which constraints interference to the contribution of two consecutive blocks of M symbols. We see that full convergence between the FTN system and the orthogonal coded system is not achieved using zero-forcing equalization. This can be explained by the fact that the zero-forcing strategy considered here yields a noise amplification at the output of the feedforward filter, before the SISO converter in Figure 4. As a result, even if perfect *a priori* estimates are available, this is, no residual IPI is present at the input of the equalizer, the noise amplification yields suboptimal performance results with respect to the orthogonal system at the Nyquist rate.

EXIT simulations represent input-output relations of average mutual information between LLRs and input symbols for a given block (equalizer or decoder), denoted $I(L_A, c_{m,n})$ and $I(L_E, c_{m,n})$. Figure 7 predicts better convergence performance for rectangular pulse shapes than for OBE pulse shapes, as previously shown by BER simulations, three to four iterations being needed to reach the iterative convergence. A higher equalizer/decoder convergence point (intersection between plain and dashed lines) is confirmed in the rectangular case.

The impact of density on system performance is depicted in Figure 8. We remark the BER being an almost linear function of ρ for both rectangular and OBE pulse shapes. In addition to system performance for $\rho = 1.5$, illustrated in previous figures, the system performs a BER $\simeq 6 \cdot 10^{-6}$ using rectangular pulse shaping for $\rho = 1.25$.

V. CONCLUSION

In this paper, we have shown a complete multicarrier faster-than-Nyquist system based on short-length filters. The latter assumption allows a very low-complexity implementation of the system while achieving good performance over an AWGN channel. Therefore, a density gain of 50% compared to the orthogonal system is achieved by means of zero-forcing turbo equalization. In addition, one notes the impact of pulse shaping on the multicarrier block, rectangular filters yielding better performance over the AWGN channel. On the other hand, we have shown that the iterative zero-forcing receiver yields suboptimal performance due to noise amplification in the iterative process.
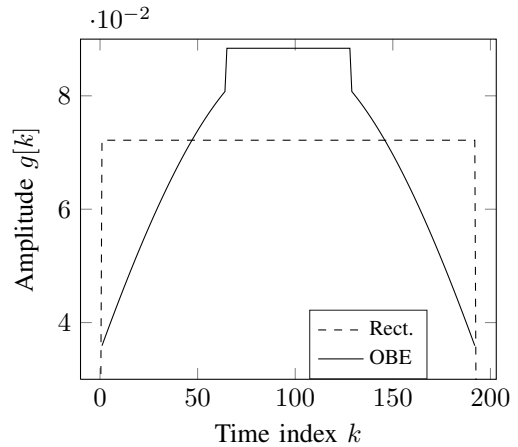

Fig. 5.   Time domain representation of rectangular and out-of-band energy (OBE) minimization pulse shaping filters.
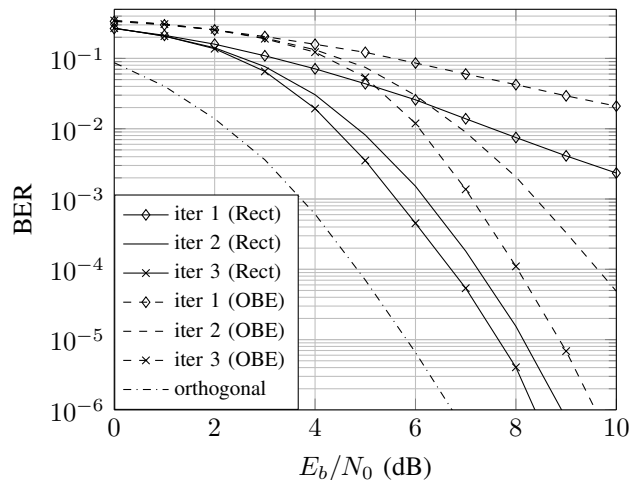

Fig. 6.   BER performance as a function of E_b/N_0 with $M = 192$, $N = 128$, $\rho = 1.5$ and $K = 2048$.

Further work on faster-than-Nyquist multicarrier systems may consider convolutive channel models, where non-rectangular pulse shaping might be of interest in order to limit interference, in particular in the presence of channel estimation errors.

REFERENCES

[1] J. E. Mazo, "Faster-than-Nyquist signaling," *Bell. Syst. Tech. Journal*, vol. 54, pp. 1451–1462, Oct. 1975.
[2] G. Forney, "Maximum-likelihood sequence estimation of digital sequences in the presence of intersymbol interference," *Information Theory, IEEE Transactions on*, vol. 18, no. 3, pp. 363–378, 1972.
[3] M. Tüchler and A. Singer, "Turbo equalization: An overview," *Information Theory, IEEE Transactions on*, vol. 57, no. 2, pp. 920–952, 2011.
[4] J. Anderson, F. Rusek, and V. Owall, "Faster-than-Nyquist signaling," *Proceedings of the IEEE*, vol. 101, no. 8, pp. 1817–1830, Aug 2013.
[5] F. Rusek and J. Anderson, "Multistream faster than Nyquist signaling," *Communications, IEEE Transactions on*, vol. 57, no. 5, pp. 1329 –1340, may 2009.
[6] D. Dasalukunte, F. Rusek, and V. Owall, "An iterative decoder for multicarrier faster-than-Nyquist signaling systems'," in *IEEE International Communication Conference*, 2010.
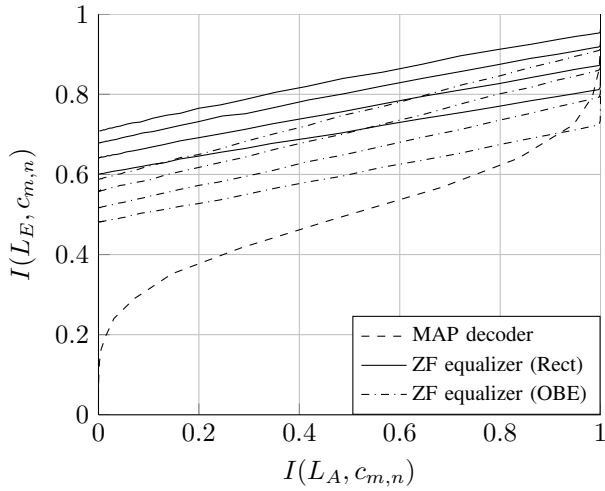
Fig. 7. EXIT chart for $E_b/N_0 = 6, 7, 8, 9$ dB (from bottom to top) with $M = 192$, $N = 128$, $\rho = 1.5$ and $K = 2048$.
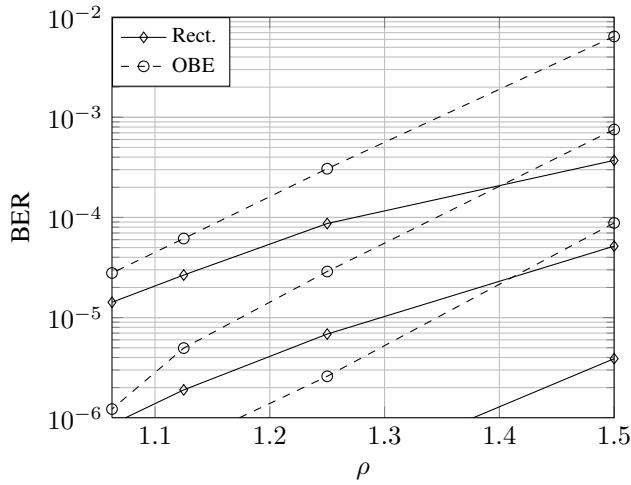

Fig. 8. BER performance as a function of ρ after 3 iterations for $E_b/N_0 = 6, 7, 8$ dB (from top to bottom), $N = 128$ and $K = 2048$.

via Weyl-Heisenberg frames over time-frequency dispersive channels," *Communications, IEEE Transactions on*, vol. 57, no. 6, pp. 1721–1733, 2009.

[15] C. Siclet, P. Siohan, and D. Pinchon, "Perfect reconstruction conditions and design of oversampled DFT-modulated transmultiplexers," *EURASIP journal on applied signal processing*, vol. 2006, pp. 1–14, 2006.

[16] R. Koetter, A. Singer, and M. Tuchler, "Turbo equalization," *Signal Processing Magazine, IEEE*, vol. 21, no. 1, pp. 67–80, Jan 2004.

[17] J. Hagenauer, "The EXIT chart - introduction to extrinsic information transfer in iterative processing," in *Proc. 12th Europ. Signal Proc. Conf (EUSIPCO*, 2004, pp. 1541–1548.

[7] D. Dasalukunte, F. Rusek, J. Anderson, and V. Owall, "Design and implementation of iterative decoder for faster-than-Nyquist signaling multicarrier systems," in *VLSI (ISVLSI), 2011 IEEE Computer Society Annual Symposium on*, july 2011, pp. 359 –360.

[8] F. Schaich and T. Wild, "A reduced complexity receiver for multicarrier faster-than-Nyquist signaling," in *Proc. IEEE GLOBECOM 2013 Workshop-Broadband Wireless Access*, 2013.

[9] "Mobile and Wireless communications enabler for the twenty-twenty information society'," https://metis2020.com.

[10] D. Roque and C. Siclet, "Performances of weighted cyclic prefix OFDM with low-complexity equalization," *IEEE Commun. Lett.*, vol. 17, no. 3, pp. 439–442, 2013.

[11] D. Pinchon and P. Siohan, "Closed-form expressions of optimal short PR FMT prototype filters," in *Global Telecommunications Conference (GLOBECOM 2011), 2011 IEEE*, Dec 2011, pp. 1–5.

[12] C. Siclet, P. Siohan, and D. Pinchon, "Oversampled orthogonal and biorthogonal multicarrier modulations with perfect reconstruction," in *Digital Signal Processing, 2002. DSP 2002. 2002 14th International Conference on*, vol. 2, 2002, pp. 647–650 vol.2.

[13] O. Christensen, *Frames and bases: An introductory course*. Birkhauser, 2008.

[14] F.-M. Han and X.-D. Zhang, "Wireless multicarrier digital transmission